Online Efficiency Optimization of a Switched Reluctance Generator in Single-Pulse Operating Mode

Šime Grbin and Dinko Vukadinović *

Posted Date: 6 May 2026

doi: 10.20944/preprints202605.0371.v1

Keywords: switched reluctance generator; losses; efficiency; P&O method

 doi:10.20944/preprints202605.0371.v1

Article

Online Efficiency Optimization of a Switched Reluctance Generator in Single-Pulse Operating Mode

Šime Grbin [1] and Dinko Vukadinović [2,*]

[1] HEP-ODS Elektra Zadar, 23000 Zadar, Croatia

[2] Faculty of Electrical Engineering, Mechanical Engineering and Naval Architecture, Department of Power Engineering, University of Split, 21000 Split, Croatia

* Correspondence: dvukad@fesb.hr

Abstract

This paper presents a method for continuously optimizing the turn-on and turn-off angles of a switched reluctance generator (SRG) operating in single-pulse mode and connected to an asymmetric bridge converter. The optimal angles are defined as those that minimize total SRG loss while ensuring accurate tracking of the terminal voltage reference. The Pearson correlation coefficient between SRG loss and selected SRG variables was calculated, with the highest correlation found for the average value of all phase currents. Therefore, the average phase current was selected as the variable to be minimized in a perturb-and-observe (P&O) method used to determine the optimal turn-on angle at a given operating point. The turn-off angle was calculated to maintain the terminal voltage at its reference value. The method was validated using both a conventional SRG simulation model and an advanced model that accounts for mutual coupling, iron losses, and remanent magnetism, and was further verified experimentally on an 8/6 SRG rated at 1.1 kW under various load conditions, terminal voltages, and rotor speeds.

Keywords: switched reluctance generator; losses; efficiency; P&O method

1. Introduction

Switched reluctance generators (SRGs) have attracted significant attention in variable-speed energy conversion systems due to their simple and robust construction, lack of rotor windings and permanent magnets, high fault tolerance, and ability to operate over a wide speed range [1–3]. These features make SRGs suitable for applications such as wind energy conversion systems, hybrid and electric vehicles, and other variable-speed generation systems where reliability, low material cost, and operation under harsh conditions are important [4,5]. However, SRG control remains challenging because the electromagnetic energy conversion process depends strongly on rotor position and phase current, and the machine exhibits pronounced magnetic nonlinearity.

When the generator operates above base speed, SRGs are typically controlled in single-pulse mode, where each phase is excited once per electrical cycle. In this regime, generator performance is primarily determined by the switching-angle pair, consisting of the turn-on and turn-off angle. These angles define the conduction interval of the phase current and directly affect generated power, phase-current waveforms, terminal current, torque ripple, and total system losses [6–8]. As a result, determining appropriate switching angles has become a central issue in SRG control.

One line of research addresses this problem using analytical or model-based approaches. A linear SRG model was used in [6] to determine the switching angles online in the single-pulse operating region, setting the turn-off angle for efficiency optimization and adjusting the turn-on angle to control generated power. In [7], analytical relations were derived for determining optimal turn-on and turn-off angles from flux-linkage characteristics and operating conditions to maximize energy-

 doi:10.20944/preprints202605.0371.v1

conversion efficiency while maintaining the desired dc-link voltage. More recently, the authors in [9] proposed a linear normalized model to analyze the influence of the turn-on angle on SRG performance and determine its optimal value using the energy conversion ratio and the peak-to-peak terminal voltage ripple. However, in that study, the terminal voltage is controlled at a fixed value of 48 V, which restricts the analysis to a single electrical operating condition.

Another important group of studies determines the switching angles using optimization-based approaches. In [10], an optimization framework was proposed based on the design of computational experiments and response surface modeling to maximize efficiency and minimize torque ripple in SRG-based wind energy systems. The authors in [5] also applied multiobjective optimization in the context of regenerative braking of electric vehicles, where the switching angles were obtained using a weighted objective function that combined generated power, torque smoothness, and current smoothness. In [11], switching-angle optimization in single-pulse operation was investigated by proposing two methods to determine the switching-angle pair required to produce a specified output power while minimizing either the phase RMS current or the terminal RMS current. Additionally, [12] analyzed the role of control objectives in SRG generating mode and showed that the resulting conduction angles depend on the selected optimization criterion. In a related direction, [13] investigated excitation control in single-pulse operation and analyzed the placement of the excitation interval within the inductance profile to improve generator efficiency while maintaining stable terminal voltage. This optimization-oriented approach was also presented in [4] with a control strategy for SRGs in wind energy systems capable of operating over a wide speed range. In that study, the analysis was performed for a constant DC-link voltage of 400 V, and the conventional SRG simulation model was used. The switching angles were determined by processing simulation results through minimization of a cost function. The variables included in the cost function are torque ripple, average phase current, and maximum flux linkage. A closely related paper [14] investigated SRG control using direct control of the average electromagnetic torque. In that approach, the switching angles are obtained from offline optimization results stored in look-up tables that provide a compromise between torque ripple reduction and efficiency improvement. Additionally, the authors used an artificial neural network to estimate the average electromagnetic torque required by the control algorithm.

Another approach determines the switching angles indirectly using control strategies or estimation methods. In [15], a voltage-control strategy was proposed in which the DC bus voltage is controlled in an outer loop, while the average phase current is controlled in an inner loop, so the resulting switching angles are determined by the voltage and current control. An artificial neural network was used in [16] to estimate the switching angles from the reference output power and rotor speed, replacing explicit optimization with a trained nonlinear mapping.

In addition to switching-angle determination, several studies have examined how converter operation and excitation strategies affect SRG performance. The authors in [17] analyzed the influence of freewheeling intervals on single-pulse operation and showed that the resulting current evolution depends not only on the commanded switching angles but also on the converter freewheeling paths. A comparison of single-pulse, current-chopping, and voltage-PWM operation in both motoring and generating modes was presented in [18], demonstrating that the selected operating mode significantly affects current waveforms and energy-conversion characteristics.

To the best of the authors' knowledge, only a very limited number of SRG studies have considered perturb-and-observe (P&O) or closely related perturbation-based optimization methods in connection with switching-angle control. The authors in [19] applied a perturb-and-observe strategy for maximum efficiency point tracking, where the turn-on angle was first selected and kept fixed, while the turn-off angle was subsequently perturbed to improve the generator efficiency. More recently, [20] proposed an extremum-seeking-based maximum power extraction strategy, in which the switching angles were parameterized in terms of the center and width of the conduction interval. Unlike these previous approaches, the method proposed in this paper does not couple the turn-on and turn-off angles through a prescribed algebraic relation. This provides greater freedom in

 doi:10.20944/preprints202605.0371.v1

selecting the switching angles and enables a broader search for the minimum-loss operating condition.

The accuracy of switching-angle determination is strongly affected by the fidelity of the adopted SRG model. The authors in [8] developed and experimentally verified a model of a single-pulse-operated SRG that can be used to analyze generator dynamics in this operating region. This modeling approach, which uses a small-signal model, was later extended in [21]. More recently, an advanced SRG model incorporating mutual coupling, iron losses, and remanent magnetism was introduced in [22], enabling a more realistic representation of the generator's electromagnetic behavior and loss mechanisms.

Despite extensive literature on switching-angle determination in SRGs, many reported approaches rely on simplified machine models that neglect important physical effects such as mutual coupling, iron losses, and remanent magnetism. Consequently, the relationship between switching angles, phase currents, and total system losses may not be accurately represented, especially when the generator operates over a wide range. To address this, this paper investigates the efficiency characteristics of a switched reluctance generator operating in single-pulse mode using an advanced SRG model that includes mutual coupling, iron losses, and remanent magnetism. The analysis reveals a strong Pearson correlation between minimum total system losses and minimum average phase current. Based on this finding, the optimal operating point can be identified through the average phase current, which can be directly measured during generator operation. The proposed approach is evaluated using both a conventional SRG model and the advanced model described in [22], and is experimentally validated on an 8/6 SRG rated at 1.1 kW under different operating conditions and over a wide terminal voltage range from 150 V to 300 V.

2. SRG Control

The operation of an SRG requires a power electronic converter. The asymmetric bridge converter is the most commonly used topology. Figure 1 shows the converter in a four-phase SRG configuration together with the load resistance R_l and the capacitor C, which supplies the energy required for the magnetization of the phase windings.

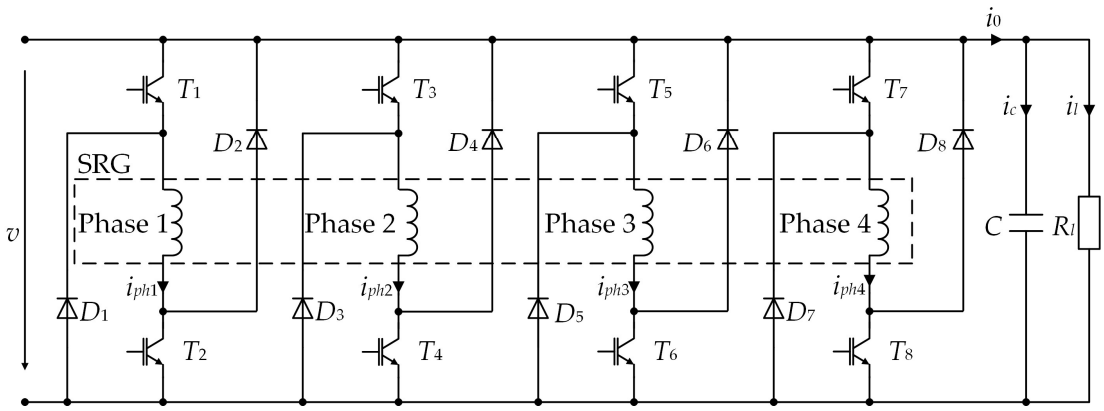

Figure 1. Equivalent circuit of the four-phase SRG connected to the asymmetric bridge converter and the load resistance.

In this paper, each SRG phase and its converter operate in two stages: magnetization and demagnetization, as shown in Figure 2. Under these conditions, when the induced EMF exceeds the terminal voltage, the phase current continues to increase even after the magnetization interval. Magnetization begins at θ_{on}, when both transistors in the same converter leg are turned on, and ends at θ_{off}, when they are turned off. During this interval, the terminal voltage is applied to the phase, and the phase current increases. After turn-off, the diodes in the same leg conduct the phase current while the phase inductance decreases. During this interval the phase current rise even after θ_{off}, which can

 doi:10.20944/preprints202605.0371.v1

lead to a large uncontrolled phase current peak. Figure 2 also shows the cross-section of the 8/6 SRG with the rotor at the aligned position (θ_a) and the unaligned position (θ_u).

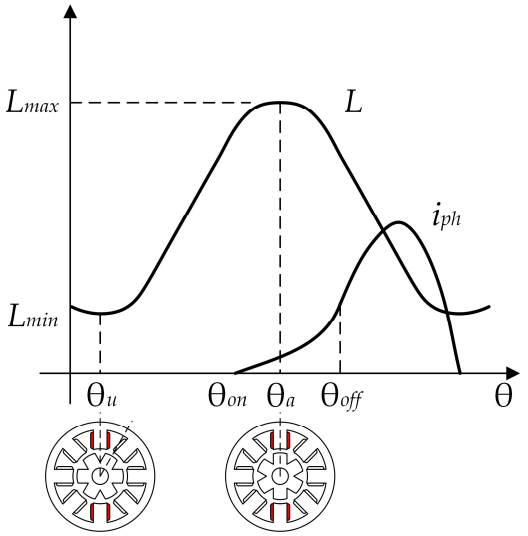

Figure 2. Magnetization and demagnetization of an SRG phase with SRG cross-section in aligned and unaligned positions.

To avoid high phase current peaks, the SRG terminal voltage can be controlled as shown in Figure 3. As in [22], the terminal voltage is the controlled variable and the magnetization angle is the output of the PI controller this paper. However, the difference lies in the determination of θ_{on}. In the proposed approach, θ_{on} is obtained using a P&O method aimed at minimizing the sum of the SRG copper and iron losses based on the measured currents of all SRG phases, the terminal voltage, and the reference terminal voltage.

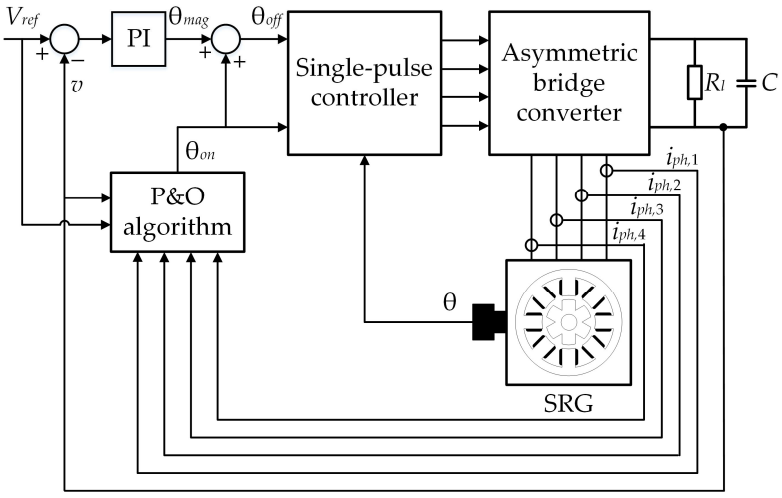

Figure 3. SRG terminal voltage control system.

The single-pulse controller shown in Figure 3 determines the switching instants of the transistors in the same converter leg. If the rotor position is between θ_{on} and θ_{off}, the two transistors in the same leg are switched on; otherwise, they are switched off. The main purpose of the control system shown in Figure 3 is to minimize the SRG loss (i.e., maximize the SRG efficiency) while maintaining the desired terminal voltage.

 doi:10.20944/preprints202605.0371.v1

3. Advanced Mathematical Model of the SRG

A conventional SRG model does not provide accurate efficiency modeling, mainly because it neglects iron losses, which can account for up to 50% of the total loss. Therefore, this paper uses an advanced mathematical model of the SRG that includes iron losses, mutual inductances, and remanent magnetism. The advanced SRG model is described in detail in [22] and is briefly presented in this section.

Figure 4 shows the equivalent circuit of one SRG phase, which forms the basis for the advanced SRG model. This model includes iron losses, the EMF due to mutual coupling e_m, the EMF due to remanent magnetism e_r, and the switching elements of the asymmetric bridge converter. Of the remaining elements in Figure 4, R represents the winding resistance, L the phase inductance, and R_{Fe} the iron-loss resistance.

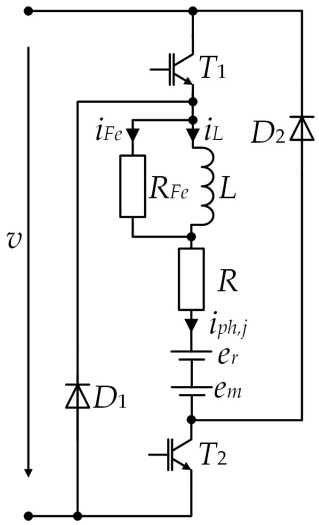

Figure 4. Advanced SRG equivalent circuit of one phase with switching elements of the asymmetric bridge converter

The following equation applies to the phase current i_{ph}:

$$i_{ph} = i_L + k i_{Fe} \tag{1}$$

where k denotes the switching state of the transistors.

During magnetization, k = 1 and the transistors shown in Figure 4 are switched on, whereas during demagnetization, k = −1 and the transistors are switched off. The following equation applies to the equivalent circuit shown in Figure 4:

$$kv = Ri_{ph} + \frac{d\psi}{dt} + e_r + e_m \tag{2}$$

The flux-linkage, from (2), is

$$\psi = \int_0^t (kv - Ri_{ph} - e_r - e_m)dt + \psi(0) \tag{3}$$

Since the SRG operates in single-pulse mode, the flux-linkage at the time the transistors are switched on is 0 Wb, i.e. $\psi(0)$ = 0 Wb.

The DC excitation experiment was used to determine the current through the inductance and the current through the iron loss resistance for a given flux-linkage and position. The dependencies of the current i_L and i_{Fe} on the position and the flux-linkage are shown in Figures 5 and 6.

 doi:10.20944/preprints202605.0371.v1

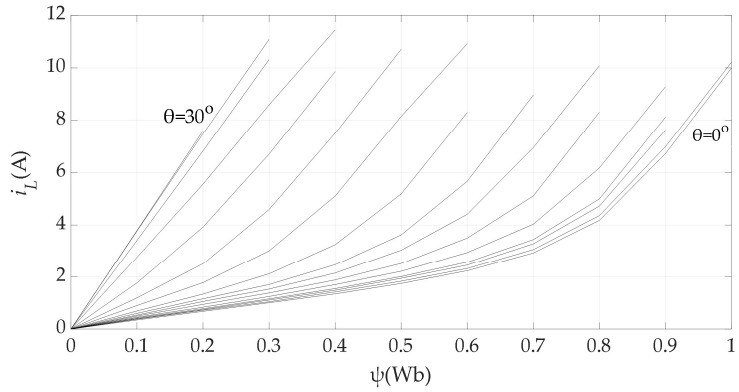

Figure 5. Inductance current versus flux-linkage for different rotor positions.

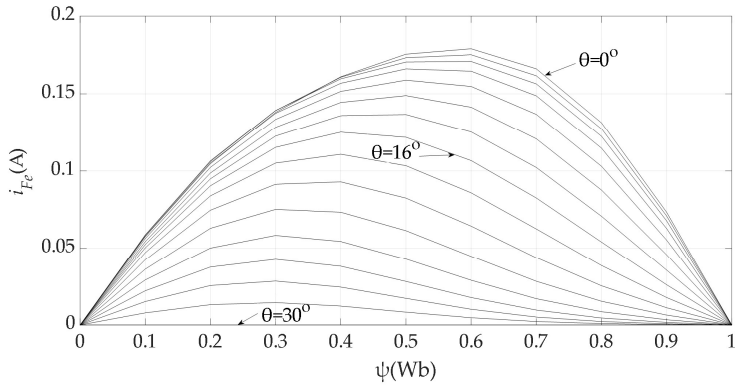

Figure 6. Iron loss resistance current versus flux-linkage for different rotor positions.

Finally, the flux-linkage calculated using (3), together with the rotor position θ, is used to determine the inductance current i_L and the current through the iron-loss resistance i_{Fe}, based on the data shown in Figures 5 and 6 and stored in look-up tables.

Due to mutual coupling between the SRG phases, part of the flux-linkage of a neighboring phase is linked with the phase under consideration. In [22], it was shown that for mutual coupling modeling, it is sufficient to consider only the coupling between a given phase and the previously magnetized phase. The direction of the flux-linkage in each phase is important. The portion of the phase-2 flux-linkage coupled with phase 1 is opposite in direction to the flux-linkage of phase 1. The same applies to phase 3 with respect to phase 2 and to phase 4 with respect to phase 3. In contrast, the portion of the phase-4 flux-linkage coupled with phase 1 has the same direction as the flux-linkage of phase 1. The flux in a given phase caused by the j^{th} phase current is therefore given by

$$\begin{aligned} \psi_{j-1,j} &= i_{phj}M, j = 2,3,4 \\ \psi_{j+3,j} &= -i_{phj}M, j = 1 \end{aligned} \tag{4}$$

where M is the mutual inductance between a certain phase and previously magnetized phase.

The experimentally determined mutual inductance and its polynomial interpolation are shown in Figure 7.

 doi:10.20944/preprints202605.0371.v1

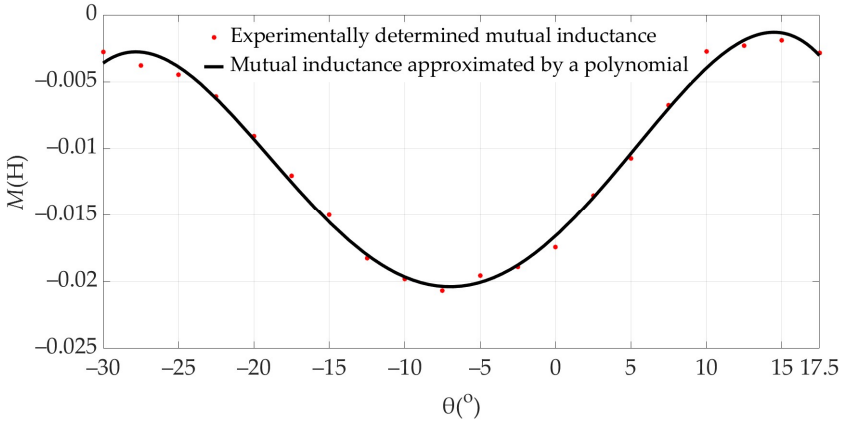

Figure 7. Mutual inductance between a certain phase and previously magnetized phase.

The equation of the polynomial describing the mutual inductance shown in Figure 7 is as follows:

$$M = \sum_{l=0}^{4} m_l \theta^l \tag{5}$$

where the polynomial coefficients are $m_0 = -1.65 \cdot 10^{-2}$, $m_1 = 1.03 \cdot 10^{-3}$, $m_2 = 5.67 \cdot 10^{-5}$, $m_3 = -2.48 \cdot 10^{-6}$, $m_4 = -9.16 \cdot 10^{-8}$ determined using the Matlab Basic Fitting Tool.

By differentiating the flux linkages in (4) with respect to time and considering (5), the induced EMF caused by the j^{th} phase is calculated as follows:

$$e_m = \begin{cases} e_{j-1,j} = \dfrac{d\psi_{j-1,j}}{dt} = \dfrac{di_{phj}}{dt} M + i_{phj} \dfrac{dM}{dt} = \dfrac{di_{phj}}{dt} M + i_{phj} \dfrac{dM}{d\theta} \dfrac{d\theta}{dt} = \\ \quad = \dfrac{di_{phj}}{dt} \sum_{l=0}^{4} m_l \theta^l + i_{phj} \sum_{l=0}^{4} l m_l \theta^{l-1} \dfrac{180^\circ}{\pi} \omega, \quad j = 2,3,4 \\ e_{j+3,j} = \dfrac{d\psi_{j+3,j}}{dt} = -\left(\dfrac{di_{phj}}{dt} M + i_{phj} \dfrac{dM}{dt} \right) = -\left(\dfrac{di_{phj}}{dt} M + i_{phj} \dfrac{dM}{d\theta} \dfrac{d\theta}{dt} \right) = \\ \quad = -\left(\dfrac{di_{phj}}{dt} \sum_{l=0}^{4} m_l \theta^l + i_{phj} \sum_{l=0}^{4} l m_l \theta^{l-1} \dfrac{180^\circ}{\pi} \omega \right), \quad j = 1 \end{cases} \tag{6}$$

In (6), the rotor position is given in degrees. Since the rotor speed ω is given in rad/s, the factor 180/π appears in (6).

During the periodic magnetization and demagnetization of the SRG phases, remanent magnetism remains in the SRG iron. This remanent magnetism produces the remanent flux ψ_r. Only half of the total remanence is associated with the rotor, and this component is responsible for the EMF induced by the remanent flux. As shown in [22] the remanent magnetism in the rotor of the j^{th} phase of the SRG is calculated by the following equation:

$$\psi_{r,j}(\theta) = \psi_{rmax,j}(-0.033 \operatorname{sgn}(\theta)\theta + 1) \tag{7}$$

where $j = 1,\ldots,4$, $\psi_{rmax,1} = -0.5\psi_{rmax}$, $\psi_{rmax,2} = -0.5/3\psi_{rmax}$, $\psi_{rmax,3} = 0.5/3\psi_{rmax}$, $\psi_{rmax,4} = 0.5\psi_{rmax}$.

Considering (7), the induced EMF due to the remanent magnetism in the rotor for the j^{th} phase of the SRG is calculated by the following equation:

$$e_r = \frac{d\psi_{r,j}(\theta)}{dt} = \frac{d\psi_{r,j}(\theta)}{d\theta} \frac{d\theta}{dt} = \psi_{rmax,j}(-0.033 \operatorname{sgn}(\theta)) \frac{180^0}{\pi} \omega \tag{8}$$

Equation (8) applies to the rotor pole under consideration and to all other rotor poles. The EMFs calculated using (6) and (8) are then used to obtain the advanced equivalent circuit of the SRG.

 doi:10.20944/preprints202605.0371.v1

The complete diagram of the advanced model of the j^{th} phase of the SRG, which was realized in Matlab/Simulink, is shown in Figure 8.

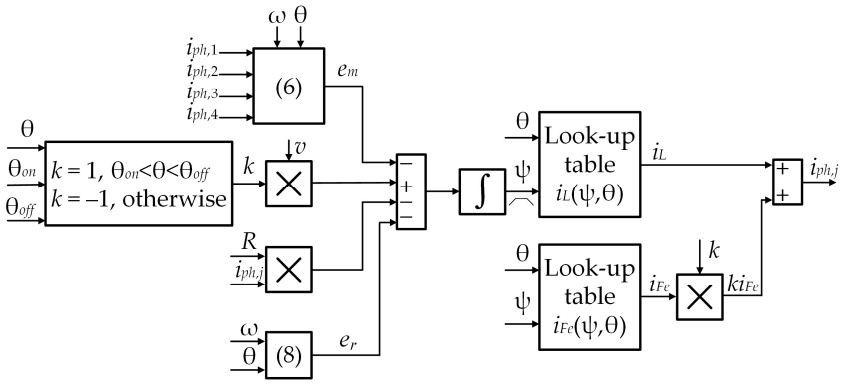

Figure 8. Diagram of the advanced model of the j^{th} phase of SRG.

The complete diagram of the advanced SRG model is obtained by superimposing the individual SRG phases, each shown in Figure 8.

4. Efficiency Maximization of the SRG

In single-pulse operation of an SRG, the turn-on and turn-off angles must be determined. Each steady-state operating point can be achieved with different turn-on and turn-off angles, and different combinations of these angles can produce the same desired value of the controlled SRG variable, allowing the selection of an optimal combination. In this paper, the controlled variable is the terminal voltage, which is controlled by varying the turn-off angle, as shown in Figure 3. The turn-on angle is adjusted using the P&O method to minimize SRG loss. Because this loss is difficult to measure accurately in real time, it is useful to identify an SRG variable that is strongly correlated with SRG loss and is relatively easy to measure. The SRG loss was determined as the difference between the measured input power and the output power dissipated in the load resistor R_l. The input power was obtained by subtracting the mechanical losses from the product of the measured mechanical torque and the rotor speed. In this way, the mechanical losses were not included in the SRG model itself; however, they were still taken into account.

The following section describes the selection of predefined SRG variables (hereinafter referred to as candidate variables) that can be easily determined during machine operation and the evaluation of their correlation with the SRG loss.

4.1. Correlation Between SRG Variables and Loss

As discussed in Section 1, various approaches have been proposed for optimizing the turn-on and turn-off angles in the single-pulse operation of an SRG. In this paper, SRG variables sensitive to measurement noise, such as torque ripple and peak magnetic flux [10,13], as well as dc-link current ripple [23], are not considered. The candidate variables considered were the average value of the excitation penalty for all phases, ε, together with the average value, I_{phAV}, and the RMS value, I_{phRMS}, of all phase currents. To determine the correlation between the selected candidate variables and the SRG loss, a series of experiments was conducted on a laboratory prototype.

Similar to [22], combinations of rotor speeds of 2000 rpm and 3000 rpm, terminal voltages of 150 V, 200 V, 250 V, and 300 V, and load resistances of 110 Ω, 65 Ω, and 45 Ω were used. However, unlike in [22], the turn-on angle was manually varied from −15° to a maximum of 5° in steps of 2°. It should be emphasized that, for some steady-state operating points, it was neither possible nor necessary to maintain steady-state SRG operation at a turn-on angle of 5°, since a sufficiently high magnetic flux could not be established. In this way, a total of 166 steady-state SRG operating points were obtained.

 doi:10.20944/preprints202605.0371.v1

The SRG loss was determined as the difference between the measured input power and the output power dissipated in the load resistor R_l. The measured points are marked by circles, while the plotted curves represent third-order polynomial interpolations shown for illustration only.

Figure 9 shows ten of these steady-state operating points: SRG loss (a), average RMS value of all phase currents (b), average value of all phase currents (c), and average excitation penalty (d), all as functions of the turn-on angle at 3000 rpm, V_{ref} = 300 V, and R_l = 110 Ω.

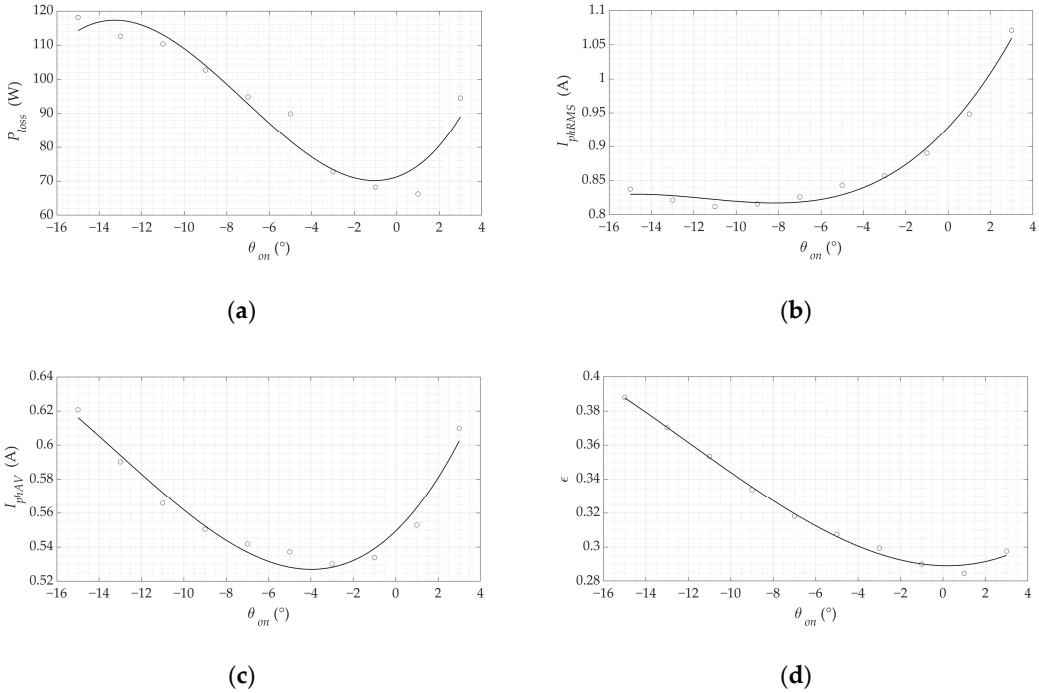

Figure 9. SRG loss (a), average RMS value of all phase currents (b), average value of all phase currents (c), and average excitation penalty (d) as functions of the turn-on angle at 3000 rpm, V_{ref} = 300 V, and R_l = 110 Ω.

As shown in Figure 9, the minimum SRG loss were obtained at a turn-on angle of 1°, which also corresponds to the minimum of average excitation penalty. This minimum was achieved at the same turn-on angle, as shown in Figure 9(d). It is important to note that the SRG efficiency at a turn-on angle of 1° is 89.6%, whereas a turn-on angle of −15° results in an efficiency of 82.8%.

However, this is not necessarily the case for other steady-state operating points. For example, Figure 10 shows seven steady-state operating points: SRG loss (a), average RMS value of all phase currents (b), average value of all phase currents (c), and average excitation penalty (d), all as functions of the turn-on angle at 2000 rpm, V_{ref} = 150 V, and R_l = 45 Ω. As shown in Figure 10(a), the minimum SRG loss occurred at a turn-on angle of −7°, which also corresponds to the minimum average phase current in Figure 10(c). In this case, SRG efficiency at a turn-on angle of −7° is 80.5%, whereas a turn-on angle of −15° results in an efficiency of 79%.

 doi:10.20944/preprints202605.0371.v1

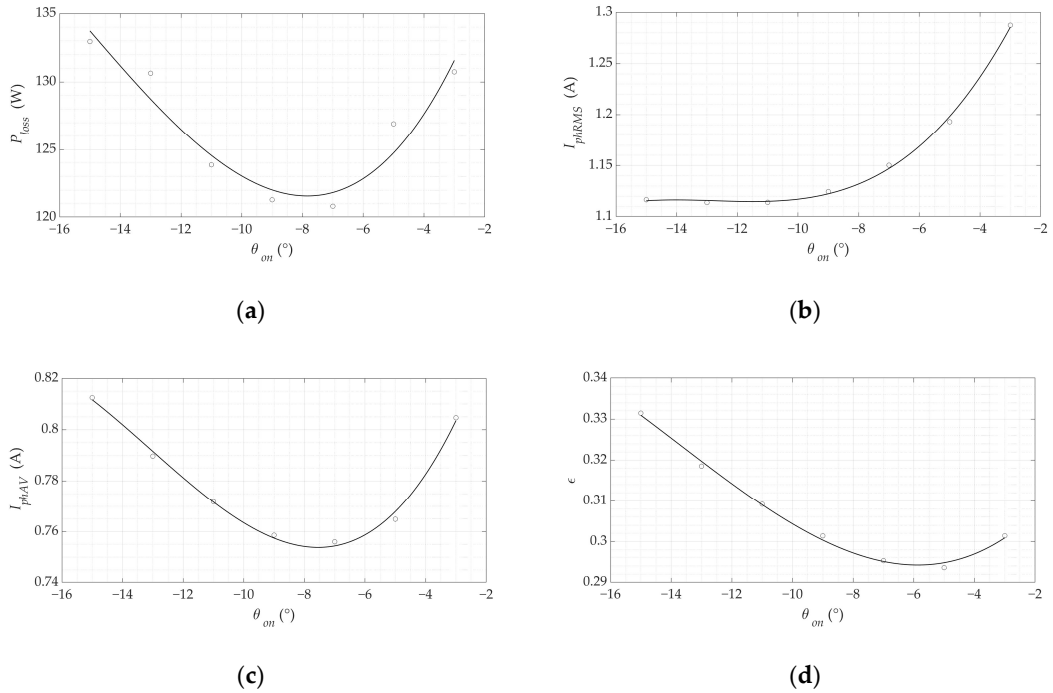

Figure 10. SRG loss (a), average RMS value of all phase currents (b), average value of all phase currents (c), and average excitation penalty (d) as functions of the turn-on angle at 2000 rpm, V_{ref} = 150 V, and R_l = 45 Ω.

The efficiency analysis of the SRG over all 166 steady-state operating points shows that a proper selection of the turn-on angle increases efficiency by 0.1% to 6.8% compared with a turn-on angle of −15°, with an average increase of 4.2%. The turn-on angle of −15° was chosen because it provides the highest magnetizing energy, allowing the largest number of steady-state operating points to be achieved without risk of demagnetization.

Therefore, depending on the operating point, the minimum SRG loss is achieved near the minimum of different candidate variables. To determine which of the analyzed variables correlates best with the minimum SRG loss, the following Pearson correlation coefficient was used [24]:

$$r_{P_{loss},J} = \frac{\sum_{k=1}^{N}((J(k)-\bar{J})(P_{loss}(k)-\bar{P}_{loss}))}{\sqrt{\sum_{k=1}^{N}((J(k)-\bar{J})^2\sum_{k=1}^{N}(P_{loss}(k)-\bar{P}_{loss})^2}} \quad (9)$$

where $J(k)$ is the candidate variable used to track the total SRG loss at the k^{th} steady-state operating point, $\bar{J}$ is the mean value of J, $\bar{P}_{loss}$ is the mean value of P_{loss}, $P_{loss}(k)$ is the total SRG loss at the k^{th} steady-state operating point, and N is the total number of analyzed steady-state SRG operating points.

The statistical significance of the Pearson correlation coefficients computed according to (9) was assessed using a two-tailed test. As the analysis included N = 166 steady-state operating points, the number of degrees of freedom was $df = N-2 = 164$. At the significance level α=0.05, the critical value of the Pearson correlation coefficient was $(r_{P_{loss},J})_{crit} = 0.152$. Thus, correlations with $|r_{P_{loss},J}| > 0.152$ were considered statistically significant at the 5% level. This criterion indicates whether the correlation is statistically different from zero, whereas the strength of the linear association with the total SRG loss was evaluated by the magnitude of $r_{P_{loss},J}$.

 doi:10.20944/preprints202605.0371.v1

The experimental results show that I_{phAV} and I_{phRMS} are strongly correlated with the total SRG loss, yielding Pearson correlation coefficients of 0.90 and 0.84, respectively, whereas ε exhibits no statistically significant linear correlation, corresponding to a coefficient of −0.07. Simulations using the advanced SRG model were also performed for the same operating points and turn-on angles, and the corresponding Pearson correlation coefficients were calculated. The simulated correlation coefficients were 0.20 for the average excitation penalty, 0.98 for the average value of all phase currents, and 0.97 for the average RMS value of all phase currents.

Therefore, both the experimental results and the advanced simulation model indicate that minimizing the average value of all phase currents leads toward the minimum-loss operating region of the SRG. Accordingly, this variable was selected to be minimized in the P&O method described in the following section.

4.2. P&O Method for Minimizing the Average Value of All SRG Phase Currents

The algorithm for maximizing the efficiency of the SRG-based system uses the P&O method, which is commonly used to determine the operating point at which a system delivers maximum power. This method has been successfully applied in wind energy conversion systems, photovoltaic systems, and similar applications [25].

The objective of this method is to find the turn-on angle that minimizes the average value of all phase currents, I_{phAV}, for a given steady-state operating point. At the same time, the magnetizing angle (and thus the turn-off angle) is determined by the PI controller to maintain the terminal voltage at its reference value, as shown in Figure 3. The PI controller used to determine the magnetizing angle operates with a period of T_{s1}=50 μs, whereas the P&O method operates with a period of T_s=0.2 s. These periods were selected experimentally, taking into account the SRG dynamics and the available processing power of the DS1104 controller board.

After each change in the turn-on angle introduced by the P&O method, a transient appears in the average value of all SRG phase currents, as shown in Figure 11(a). The turn-on angle variation is limited to ±0.5° to avoid system instability while ensuring a sufficiently fast transition to the SRG steady-state. Thus, the phase-current transient is considered settled within 0.15 s. The average value of all SRG phase currents is then calculated over the interval from 0.15 s to 0.2 s after the turn-on angle change. Figure 11(b) shows the sample counter n over the 0.2 s interval, with the spacing between successive samples equal to the sampling period of 50 μs. Accordingly, the sample counter ranges from 3001 to 4000 during the averaging interval, as shown in Figure 11(b). Figure 11(c) also shows the sample counter n_{AV} corresponding to the updates of the average value of all SRG phase currents, which changes every 0.2 s, i.e., with the same period as the P&O method.

The average value of all phase currents used in the P&O method is calculated as follows:

$$I_{phAV}(n_{AV}) = \frac{1}{1000} \sum_{n=4000(n_{AV}-1)+3001}^{4000n_{AV}} \frac{i_{ph1}(n)+i_{ph2}(n)+i_{ph3}(n)+i_{ph4}(n)}{4} \tag{10}$$

For illustration, Figure 11(a) shows the average value of all SRG phase currents, marked in red, during the last 0.05 s of the period T_s, that is, when the sample counter n_{AV} is equal to 1.

 doi:10.20944/preprints202605.0371.v1

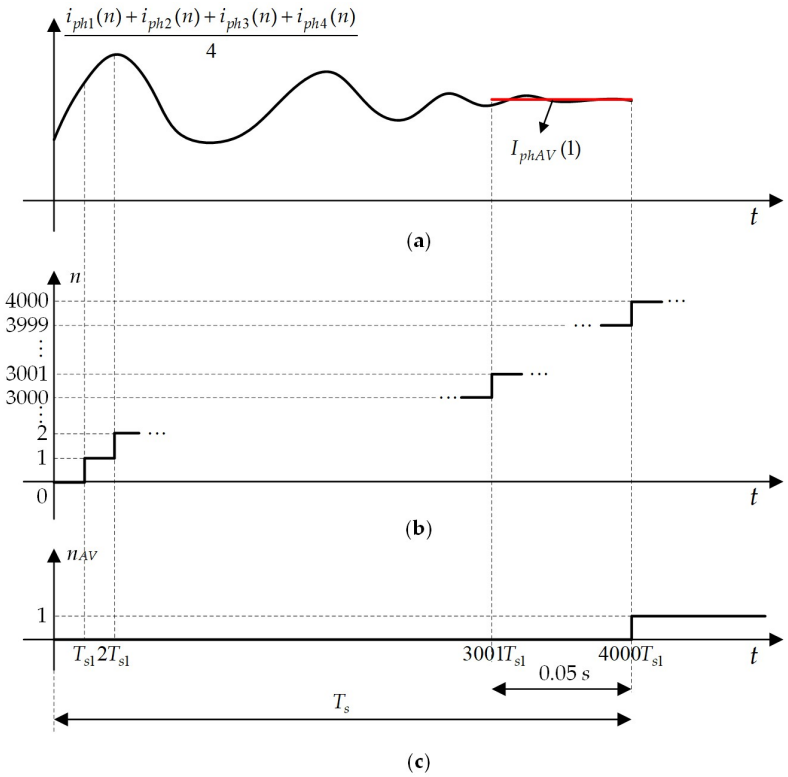

Figure 11. Average value of all SRG phase currents (a), sample counter over the 0.2 s interval (b), and sample counter of the average value of all SRG phase currents (c).

Furthermore, the change in the average value of all SRG phase currents at the n_{AV} instant, $\Delta I_{AV}(n_{AV})$, is used as an input variable of the P&O method, whereas the change in the turn-on angle at the next instant, $\Delta\theta_{on}(n_{AV}+1)$, is used to calculate the turn-on angle as the output variable of the P&O method. These quantities are calculated according to the following equations:

$$\Delta I_{phAV}(n_{AV}) = I_{phAV}(n_{AV}) - I_{phAV}(n_{AV}-1) \tag{11}$$

$$\Delta\theta_{on}(n_{AV}+1) = \theta_{on}(n_{AV}+1) - \theta_{on}(n_{AV}) \tag{12}$$

Based on the change in the average value of all phase currents using (11), and the sign of the turn-on angle change, $\mathrm{sgn}(\Delta\theta_{on}(n_{AV}))$, the magnitude and direction of the turn-on angle adjustment in the next step of the P&O method are determined. The equation used to determine the change in the turn-on angle in the next step is given by:

$$\Delta\theta_{on}(n_{AV}+1) = -k_p \Delta I_{AV}(n_{AV})\,\mathrm{sgn}(\Delta\theta_{on}(n_{AV})) \tag{13}$$

where k_p denotes the proportionality coefficient and $\Delta\theta_{on}(n_{AV}) = \theta_{on}(n_{AV}) - \theta_{on}(n_{AV}-1)$.

The proportionality coefficient k_p in (13) ensures that changes in the average value of all phase currents and changes in the turn-on angle are comparable. A small value of k_p (e.g., 10) results in a slow response of the turn-on angle variation, increasing the risk that the P&O method becomes trapped in a local minimum and ultimately fails to find the optimal turn-on angle. Conversely, a proportionality coefficient k_p significantly greater than 100 causes the turn-on angle limit of ±0.5° to be activated too frequently. Therefore, k_p was set to 100 in this paper. Even in this case, however, the method still reaches the global minimum, although with a somewhat longer settling time.

Using (12) and (13), the turn-on angle in the next step of the P&O method is calculated according to the following equation:

 doi:10.20944/preprints202605.0371.v1

$$\theta_{on}(n_{AV}+1) = -k_p \Delta I_{AV}(n_{AV}) \operatorname{sgn}(\Delta\theta_{on}(n_{AV})) + \theta_{on}(n_{AV}) \tag{14}$$

The variation of the average value of all SRG phase currents with the turn-on angle during the P&O method is shown in Figure 12.

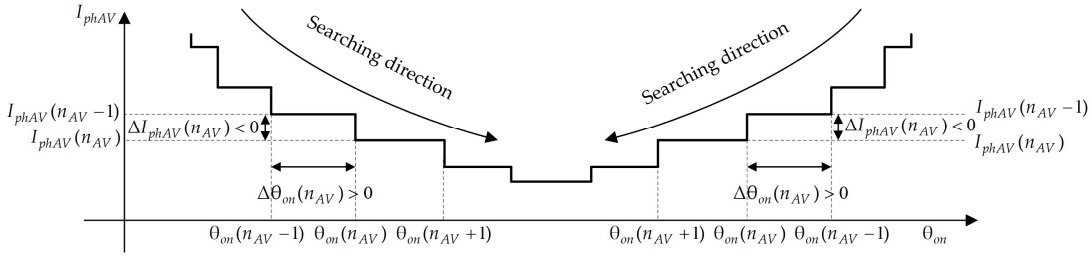

Figure 12. Average value of all SRG phase currents as a function of the turn-on angle during the P&O method.

As shown in Figure 12, if the average value of all phase currents decreases when the turn-on angle is changed from $\theta_{on}(n_{AV}-1)$ to $\theta_{on}(n_{AV})$, the turn-on angle is being varied in the correct direction, which should be retained in the next step, where the turn-on angle becomes $\theta_{on}(n_{AV}+1)$. This correct direction is denoted in Figure 12 as the "searching direction." Conversely, if the average value of all phase currents increases relative to the previous step, the turn-on angle in the next step should be changed in the opposite direction. Figure 13 shows the Matlab/Simulink model of the P&O method for average value of all SRG phase currents, with the reset function indicated by the magenta block.

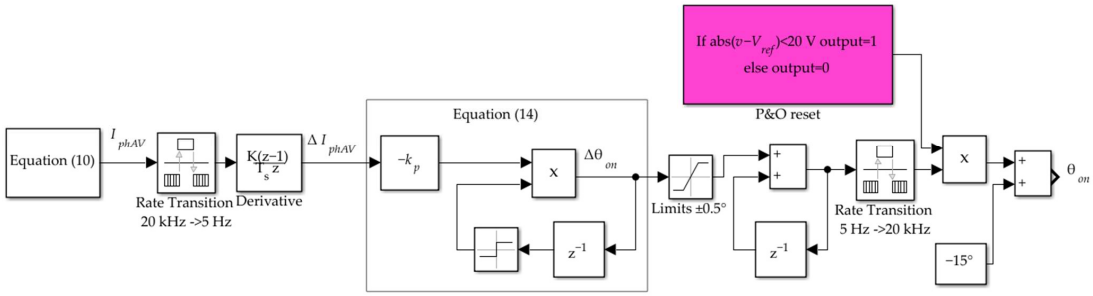

Figure 13. Matlab/Simulink model of the P&O method with the reset function.

The P&O method is activated only when the SRG has reached steady-state, as verified by continuously monitoring the absolute difference between the terminal voltage v and its reference V_{ref}. If this difference is less than 20 V, the SRG is considered to be in steady-state, and the continuous search for the optimal turn-on angle is enabled. Otherwise, the SRG is considered not to have reached steady-state, and the turn-on angle is kept at −15°.

5. Simulation and Experimental Validation of Optimal SRG Switching Angles

Figure 14(a) shows the experimental setup of the SRG control system used to evaluate the proposed P&O method, while Figure 14(b) shows a photograph of the setup.

 doi:10.20944/preprints202605.0371.v1

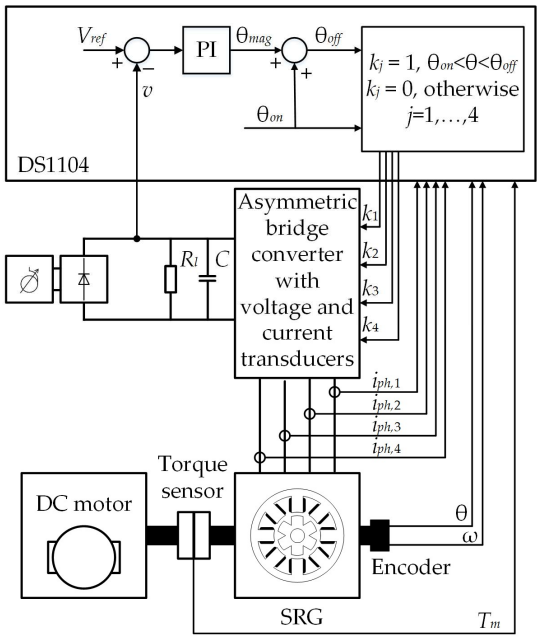

(**a**)

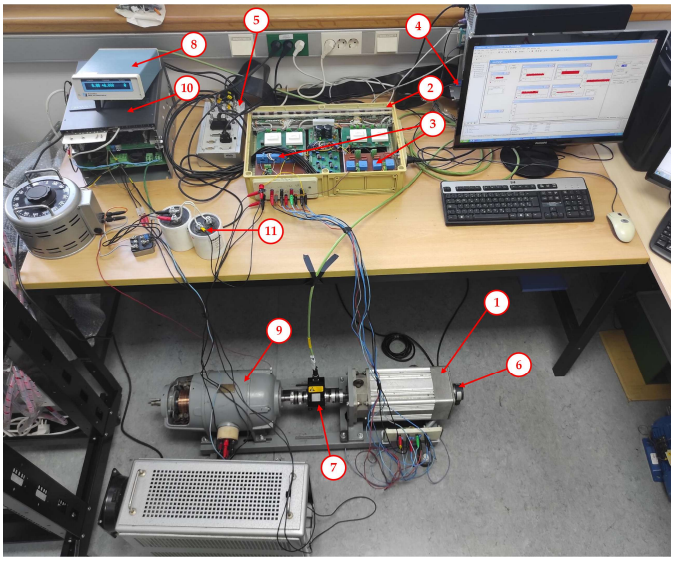

(**b**)

Figure 14. Diagram of the experimental setup of the SRG control system (a) and the photograph of the experimental setup (b).

The names and data of the main components of the experimental setup shown in Figure 14b are listed in Table 1. The parameters of the analyzed 8/6 SRG are provided in the Appendix.

The PI controller and the sampling of the measured SRG variables operate at a frequency of 20 kHz, while the P&O method operates at 5 Hz. The time-dependent variables presented in this section were stored in PC memory at 200 Hz to prevent task overruns. The PI controller parameters were determined by trial and error, with the integral gain K_i = 5 and the proportional gain K_p = 1.

 doi:10.20944/preprints202605.0371.v1

Table 1. The main components of the experimental setup and their data.

Row Number	Name	Data	Manufacturer
1	SRG	1.1 kW	Končar
2	Asymmetric bridge converter	IGBT RG4PH50UD Driver SKHI 22B	International Rectifiers Semikron
3	Hall effect transducers	LA 55-P for currents LV 25-P for voltages	LEM International
4	Controller board	DS1104	dSpace
5	Connector panel	CP1104	dSpace
6	Incremental encoder	XCC 1510PS50X	Telemecanique
7	Torque transducer	TMB 308	Magtrol
8	Torque display	3410	Magtrol
9	DC motor	1.1 kW	Winkelmann Elektromotoren
10	Power converter for DC motor	Sinamics DCM6RA813-6DV62-0AA0	Siemens
11	Electrolytic capacitors	8800 μF PEH169VN444AM	Evox Rifa

To verify the validity of the proposed P&O method, a series of experiments was carried out under both steady-state and dynamic operating conditions of the SRG. The steady-state operating points were obtained by combining rotor speeds of 2000 rpm and 3000 rpm, terminal voltages of 150 V, 200 V, 250 V, and 300 V, and load resistances of 110 Ω, 65 Ω, and 45 Ω. In this way, the SRG was tested over a wide power range, from 18.6% to 125.9% of the rated power. The dynamic transitions from one steady-state operating point to another within the aforementioned set of steady-state operating points are shown in Figures 15–18.

Figure 15 shows the responses of the selected SRG variables resulting from a step change in load resistance from 110 Ω to 65 Ω at t = 18.6 s, with the SRG operating at 3000 rpm and a reference terminal voltage of 200 V. The measured variables are shown in red, the simulated variables obtained using the advanced SRG model are shown in black, and the variables obtained using the conventional simulation model are shown in blue. Figure 15(a) shows the terminal voltage, Figure 15(b) shows the average value of all SRG phase currents, Figure 15(c) shows the turn-on angle, and Figure 15(d) shows the magnetization angle of the SRG. The step change in load resistance causes the difference between the instantaneous terminal voltage and its reference value to exceed 20 V. Whenever this occurs, the P&O method sets the turn-on angle to −15°. In the time interval from 18.6 s to 26.9 s, the algorithm attempts three times to calculate a turn-on angle different from −15°, but fails each time because $|v - V_{ref}| > 20$ V. Only after 26.9 s does $|v - V_{ref}|$ become less than 20 V, allowing the algorithm to calculate a new turn-on angle, whose average value at the newly established steady-state operating point is −7.1°.

It is important to emphasize that the magnetization angle obtained experimentally shows noticeably better agreement with the magnetization angle from the advanced simulation model, as shown in Figure 15(d). The conventional and advanced simulation models deviate by approximately the same amount from the experimentally obtained variables shown in Figures 15(a)–15(c). Notably, neither simulation model yields $|v - V_{ref}| > 20$ V during this transient, because the experimentally obtained phase currents do not fully match those from the advanced simulation model, and especially not those from the conventional simulation model. These differences are discussed in more detail in [22] and are not the focus of this paper.

 doi:10.20944/preprints202605.0371.v1

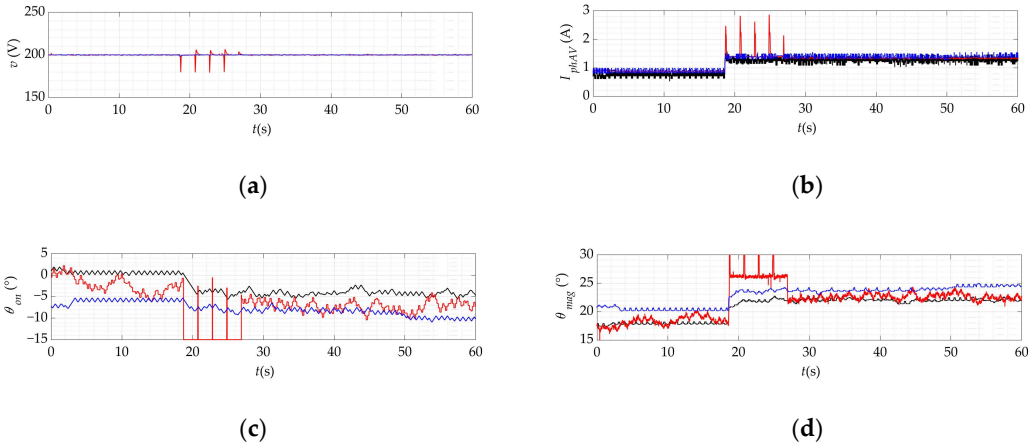

Figure 15. Dynamic response of the control system to a step change in load at 18.6 s from R_l = 110 Ω to R_l = 65 Ω at V_{ref} = 200 V and a rotor speed of 3000 rpm, showing terminal voltage (a), average phase current (b), turn-on angle (c), and magnetizing angle (d); red—experimental results, black—advanced SRG model, blue—conventional SRG model.

Figure 16 shows the dynamic response of the control system to a ramp change in rotor speed from 2000 rpm to 3000 rpm starting at 15.2 s, with V_{ref} = 150 V and R_l = 45 Ω. Figure 16(a) shows the turn-on angle, while Figure 16(b) shows the magnetization angle. The rotor speed is varied linearly over 2.5 s to prevent $|v - V_{ref}|$ from exceeding 20 V, thereby shortening the transient without affecting the optimal turn-on angles. This rotor speed variation is defined in the DC motor power converter settings. After the rotor speed change, the P&O method rapidly determines the optimal turn-on angle and the corresponding magnetization angle. Up to 15.2 s, the experimentally obtained turn-on angle agrees more closely with the result of the advanced simulation model than with that of the conventional simulation model, whereas after 15.2 s, the opposite is observed. In contrast, throughout the entire experiment, the experimentally obtained magnetization angle agrees more closely with the result of the advanced simulation model than with that of the conventional model.

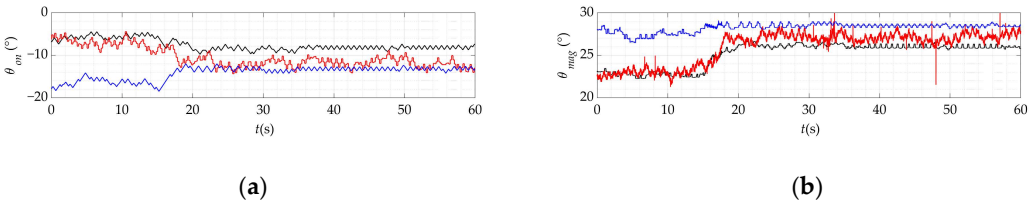

Figure 16. Dynamic response of the control system to a ramp change in rotor speed from 2000 rpm to 3000 rpm at 15.2 s at V_{ref} = 150 V and load R_l = 45 Ω, turn-on angle (a), and magnetizing angle (b); red—experimental results, black—advanced SRG model, blue—conventional SRG model.

For the dynamic operating condition shown in Figure 16, the waveforms of the terminal voltage and the average value of all SRG phase currents are not shown, as the experimental results closely match the results obtained from both simulation models. The terminal voltage ripple is less than 1.5%, while the average value of all phase currents is approximately 1.5 A before the transient (15.2 s) and 1.4 A after it ends. These values also represent the minimum average phase currents achieved at 2000 rpm and 3000 rpm, respectively.

Figure 17 shows the dynamic response of the control system to a ramp change in rotor speed from 3000 rpm to 2000 rpm, starting at 24.4 s, with V_{ref} = 150 V and R_l = 65 Ω. As in the dynamic response shown in the previous figure, the rotor speed varies linearly over 2.5 s. The waveforms of

 doi:10.20944/preprints202605.0371.v1

the terminal voltage and the average value of all SRG phase currents are not shown for the same reason stated for the dynamic response described in Figure 16. In this case, the measured average value of all phase currents changes from 1.01 A at the steady-state operating point before the transient to 1.07 A at the steady-state operating point after the transient.

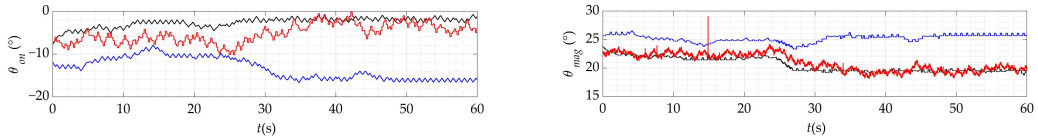

(**a**) (**b**)

Figure 17. Dynamic response of the control system to a ramp change in rotor speed from 3000 rpm to 2000 rpm at 24.4 s at V_{ref} = 150 V and load R_l = 65 Ω, turn-on angle (a), and magnetizing angle (b); red—experimental results, black—advanced SRG model, blue—conventional SRG model.

Note that the experimentally obtained waveforms of the turn-on angle (Figure 17(a)) and the magnetization angle (Figure 17(b)) agree more closely with the waveforms obtained using the advanced SRG simulation model than with those obtained using the conventional simulation model.

Finally, Figure 18 shows the dynamic response of the control system to a ramp change in V_{ref} from 300 V to 150 V, starting at 20.2 s, with 3000 rpm and R_l = 65 Ω. The rate of change of V_{ref} was set to 15 V/s to prevent activation of the P&O reset. The system would also operate with a step change in V_{ref}, but the transient would last longer. In this dynamic response, the experimentally obtained terminal voltage v closely follows the terminal voltage obtained from both simulation models, with low ripple, and is therefore not shown. In this case, the average value of all phase currents changes in steady-state from 1.94 A to 1 A, representing the minimum average values of all phase currents achieved by the P&O method.

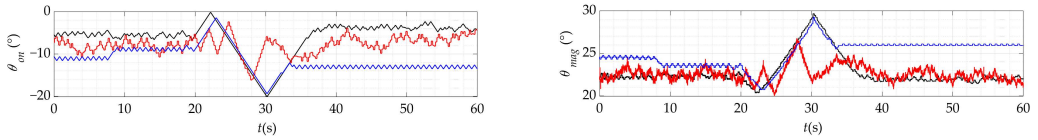

(**a**) (**b**)

Figure 18. Dynamic response of the control system to a ramp change in V_{ref} from 300 V to 150 V at 20.2 s at 3000 rpm and load R_l = 65 Ω, turn-on angle (a), and magnetizing angle (b); red—experimental results, black—advanced SRG model, blue—conventional SRG model.

6. Conclusions

This paper presents a method for continuous optimization of the turn-on and turn-off angles of a switched reluctance generator operating in single-pulse mode and supplied by an asymmetric bridge converter. In the proposed approach, the turn-on angle is optimized using the P&O method, while the turn-off angle is determined through terminal voltage control. The objective of the method is to minimize total SRG loss while maintaining the terminal voltage at its reference value.

To identify a suitable variable for real-time optimization, the correlation between SRG loss and several candidate variables was analyzed across 166 steady-state operating points. Both the experimental results and the advanced simulation model showed that the average value of all phase currents had the highest correlation with SRG loss, compared to the RMS value of the phase currents and the average excitation penalty. Based on this result, the average value of all phase currents was

 doi:10.20944/preprints202605.0371.v1

selected as the variable to be minimized by the proposed P&O method. In this way, an average efficiency increase of 4.2% was achieved compared with a turn-on angle of −15°.

The proposed method was validated by simulations and experiments on an 8/6 SRG rated at 1.1 kW over a wide range of rotor speeds, terminal voltages, and load conditions. The results confirmed that the method is capable of tracking the operating point corresponding to minimum SRG loss in both steady-state and dynamic operating conditions. In addition, the advanced SRG model showed better agreement with the experimental results than the conventional model, particularly in the prediction of the magnetization angle, owing to the inclusion of mutual coupling, iron losses, and remanent magnetism.

Overall, the obtained results demonstrate that the proposed method provides a simple and practical way to improve the efficiency of SRG-based systems using a variable that is easy to measure and suitable for real-time implementation.

Author Contributions: Conceptualization, Š.G. and D.V.; methodology, Š.G. and D.V.; software, Š.G.; validation, Š.G. and D.V.; formal analysis, Š.G. and D.V.; investigation, Š.G. and D.V.; resources, Š.G. and D.V.; data curation, Š.G. and D.V.; writing—original draft preparation, D.V.; writing—review and editing, Š.G., and D.V.; visualization, Š.G. and D.V.; supervision, D.V.; funding acquisition, D.V. All authors have read and agreed to the published version of the manuscript.

Funding: This research received no external funding.

Data Availability Statement: The data presented in this study are available on request from the corresponding author.

Conflicts of Interest: The authors declare no conflicts of interest.

Appendix

Number of phase windings: 4
Number of stator poles: 8
Number of rotor poles: 6
Rated power: 1.1 kW
Rated current: 6 A
Base speed: 1400 rpm
Outer stator diameter: 135 mm
Inner stator diameter: 80 mm
Rotor diameter: 79.5 mm
Stator stack length: 300 mm
Stator pole arc: 22°
Rotor pole arc: 24°
Number of turns per phase: 300
Phase resistance (at 20°C): 2.89 Ω

References

1. Miller, T.J.E. *Electronic Control of Switched Reluctance Machines*; Newnes power engineering series; Newnes: Oxford Boston, 2001; ISBN 978-0-7506-5073-1.
2. Bilgin B.; Jiang J. W.; Emadi A. *Switched Reluctance Motor Drives: Fundamentals to Applications*; 1st ed.; CRC PRESS: S.l., 2022; ISBN 978-1-032-33875-0.
3. Scalcon, F.P.; Fang, G.; Filho, C.J.V.; Gründling, H.A.; Vieira, R.P.; Nahid-Mobarakeh, B. A Review on Switched Reluctance Generators in Wind Power Applications: Fundamentals, Control and Future Trends. *IEEE Access* **2022**, *10*, 69412–69427, doi:10.1109/ACCESS.2022.3187048.

 doi:10.20944/preprints202605.0371.v1

4. Barros, T.A.D.S.; Neto, P.J.D.S.; Filho, P.S.N.; Moreira, A.B.; Filho, E.R. An Approach for Switched Reluctance Generator in a Wind Generation System With a Wide Range of Operation Speed. *IEEE Trans. Power Electron.* **2017**, *32*, 8277–8292, doi:10.1109/TPEL.2017.2697822.
5. Zhu, Y.; Wu, H.; Zhang, J. Regenerative Braking Control Strategy for Electric Vehicles Based on Optimization of Switched Reluctance Generator Drive System. *IEEE Access* **2020**, *8*, 76671–76682, doi:10.1109/ACCESS.2020.2990349.
6. Sozer, Y.; Torrey, D.A. Closed Loop Control of Excitation Parameters for High Speed Switched-Reluctance Generators. *IEEE Trans. Power Electron.* **2004**, *19*, 355–362, doi:10.1109/TPEL.2003.823178.
7. Kioskeridis, I.; Mademlis, C. Optimal Efficiency Control of Switched Reluctance Generators. *IEEE Trans. Power Electron.* **2006**, *21*, 1062–1071, doi:10.1109/TPEL.2006.876827.
8. Ahmad, S.S.; Narayanan, G. Modeling of Single-Pulse Operated Switched Reluctance Generator and Its Verification. *IEEE Trans. Ind. Appl.* **2020**, *56*, 4966–4976, doi:10.1109/TIA.2020.3005586.
9. Chai, Z.; Liu, C.; Wang, T.; Zhu, X. Comprehensive Performance Improvement of SRG by Turn-ON Angle Optimization Using Linear Normalized Model. *IEEE Trans. Power Electron.* **2024**, *39*, 6327–6337, doi:10.1109/TPEL.2023.3327288.
10. Neto, P.J.D.S.; Barros, T.A.D.S.; De Paula, M.V.; De Souza, R.R.; Filho, E.R. Design of Computational Experiment for Performance Optimization of a Switched Reluctance Generator in Wind Systems. *IEEE Trans. Energy Convers.* **2018**, *33*, 406–419, doi:10.1109/TEC.2017.2755590.
11. Verma, A.; Ahmad, S.S.; Narayanan, G. Optimal Control of Single-Pulse-Operated Switched Reluctance Generator to Minimize RMS Phase and RMS DC-Bus Current. *IEEE Trans. Ind. Appl.* **2023**, 1–13, doi:10.1109/TIA.2023.3327977.
12. Zahid, A.; Bilgin, B. Determining the Control Objectives of a Switched Reluctance Machine for Performance Improvement in Generating Mode. *IEEE Open J. Ind. Appl.* **2023**, *4*, 99–110, doi:10.1109/OJIA.2023.3256364.
13. Fernando, W.U.N.; Barnes, M.; Marjanovic, O. Excitation Control and Voltage Regulation of Switched Reluctance Generators above Base Speed Operation. In Proceedings of the 2011 IEEE Vehicle Power and Propulsion Conference; IEEE: Chicago, IL, USA, September 2011.
14. Hancco Catata, E.O.; De Paula, M.V.; Dos Santos Neto, P.J.; Ruppert Filho, E.; Luque Carcasi, D.B.; Dos Santos Barros, T.A. Direct Average Torque Control of Switched Reluctance Generator. *IET Power Electron.* **2023**, *16*, 2011–2021, doi:10.1049/pel2.12521.
15. Touati, Z.; Pereira, M.; Araújo, R.E.; Khedher, A. Improvement of Steady State Performance of Voltage Control in Switched Reluctance Generator: Experimental Validation. *Machines* **2022**, *10*, 103, doi:10.3390/machines10020103.
16. Kittiratsatcha, S.; Kerdtuad, P.; Bunlaksananusorn, C. Output Power Control Using Artificial Neural Network for Switched Reluctance Generator. *Sens. Mater.* **2021**, *33*, 2427, doi:10.18494/SAM.2021.3312.
17. Burkhart, B.; Klein-Hessling, A.; Hafeez, S.A.; De Doncker, R.W. Influence of Freewheeling on Single Pulse Operation of a Switched Reluctance Generator. In Proceedings of the 2016 19th International Conference on Electrical Machines and Systems (ICEMS); IEEE: Chiba, Japan, November 2016.
18. Memon, A.A.; Bukhari, S.S.H.; Hao, C. Switched Reluctance Motoring and Generating Operation in Single Pulse, Current Chopping and Voltage PWM Modes. *Electr. Eng.* **2023**, *105*, 2817–2823, doi:10.1007/s00202-023-01854-y.
19. Araujo, W.R.H.; Reis, M.R.C.; Wainer, G.A.; Calixto, W.P. Efficiency Enhancement of Switched Reluctance Generator Employing Optimized Control Associated with Tracking Technique. *Energies* **2021**, *14*, 8388, doi:10.3390/en14248388.
20. Touati, Z.; Moretti, G.; Khedher, A.; Zaccarian, L. Control and Maximum Power Extraction of a Switched Reluctance Generator with Low Resolution Pulse-Based Position Estimation. *J. Frankl. Inst.* **2025**, *362*, 107757, doi:10.1016/j.jfranklin.2025.107757.
21. Ahmad, S.S.; Verma, A.; Narayanan, G. Small-Signal Modeling of Single-Pulse-Operated Switched Reluctance Generator and Its Verification. In Proceedings of the 2023 IEEE 3rd International Conference on Sustainable Energy and Future Electric Transportation (SEFET); IEEE: Bhubaneswar, India, August 9 2023; pp. 1–6.

 doi:10.20944/preprints202605.0371.v1

22. Grbin, Š.; Vukadinović, D.; Bašić, M. Model of a Switched Reluctance Generator Considering Iron Losses, Mutual Coupling and Remanent Magnetism. *Energies* **2025**, *18*, 2656, doi:10.3390/en18102656.
23. Narla, S.; Sozer, Y.; Husain, I. Switched Reluctance Generator Controls for Optimal Power Generation and Battery Charging. *IEEE Trans. Ind. Appl.* **2012**, *48*, 1452–1459, doi:10.1109/TIA.2012.2209850.
24. Asuero, A.G.; Sayago, A.; González, A.G. The Correlation Coefficient: An Overview. *Crit. Rev. Anal. Chem.* **2006**, *36*, 41–59, doi:10.1080/10408340500526766.
25. *Advanced Power Electronics Converters for Future Renewable Energy Systems*; Priyadarshi, N., Ed.; First edition.; CRC Press: Boca Raton, 2023; ISBN 978-1-032-34714-1.